ADVANCED ENERGY MATERIALS
www.advenergymat.de

"Water-in-Eutectogel" Electrolytes for Quasi-Solid-State Aqueous Lithium-Ion Batteries

Xu Hou, Travis P Pollard, Xin He, Leilei Du, Xiaokang Ju, Wenguang Zhao, Meirong Li, Jun Wang, Elie Paillard, Hai Lin, Jingyu Sun, Kang Xu, Oleg Borodin,* Martin Winter, and Jie Li**

The development of high safety lithium-ion batteries (LIBs) is greatly impeded by the flammability and leakage concerns of typical organic solvent-based electrolytes. As one of the alternative classes of electrolytes, hydrogel electrolytes exhibit high safety, high flexibility, low cost, and are benign to the environment. However, the narrow electrochemical stability window (ESW) of typical hydrogel electrolytes restricts the operating voltage of battery cells. Here, a new class of "water-in-eutectogel (WiETG)" electrolyte is reported, fabricated by combining a hydrogel with a "deep eutectic solvent" (LiTFSI in acetamide). The obtained WiETG electrolyte exhibits non-flammability, high ionic conductivity, and a wide ESW. $LiMn_2O_4$‖$Li_4Ti_5O_{12}$ cells with the WiETG electrolyte exhibit good cycling stability, high flexibility, and high safety. This newly developed WiETG electrolyte not only broadens the ESW of typical hydrogel electrolytes, but also opens a new perspective on future directions and guidance for the design of high safety electrolytes for flexible LIBs and beyond.

1. Introduction

The increasing demand of wearable and/or flexible electronic devices requires relevant electrochemical energy storage systems.[1] Owing to their high energy density and long cycle life, lithium-ion batteries (LIBs) seem the natural choice for these emerging markets. However, typical LIBs with flammable liquid non-aqueous electrolytes suffer from potential safety concerns such as leakage and fire, especially under extreme conditions such as high pressure and deformation, which brings notable challenges for flexible electronic applications.[2] To overcome these problems, numerous attempts have been made to substitute the organic electrolytes with safer solutions, such as inorganic solid

X. Hou, X. Ju, E. Paillard, M. Winter, J. Li
Helmholtz-Institute Muenster (HI MS)
IEK-12
Forschungszentrum Juelich GmbH
Corrensstr. 46, 48149 Muenster, Germany
E-mail: jie1.li@polimi.it

T. P. Pollard, K. Xu, O. Borodin
Battery Science Branch
Sensor and Electron Devices Directorate
US Army Research Laboratory
Adelphi, MD 20783, USA
E-mail: oleg.a.borodin.civ@army.mil

X. He
School of Chemical Engineering
Sichuan University
Chengdu 610065, P. R. China
E-mail: xinhe@scu.edu.cn

The ORCID identification number(s) for the author(s) of this article can be found under https://doi.org/10.1002/aenm.202200401.

DOI: 10.1002/aenm.202200401

L. Du, M. Li, M. Winter
MEET Battery Research Center
Institute of Physical Chemistry
University of Muenster
Corrensstr. 46, 48149 Muenster, Germany

W. Zhao, H. Lin
School of Advanced Materials
Peking University
Shenzhen Graduate School, Shenzhen 518055, P. R. China

J. Wang
Academy for Advanced Interdisciplinary Studies
Southern University of Science and Technology
Shenzhen 518055, P. R. China

E. Paillard, J. Li
Department of Energy
Politecnico di Milano
Via Lambruschini, 4, Milano, MI 20156, Italy

J. Sun
College of Energy
Soochow Institute for Energy and Materials Innovations (SIEMIS)
Jiangsu Provincial Key Laboratory for Advanced Carbon Materials and Wearable Energy Technologies
Soochow University
Suzhou 215006, P. R. China

electrolytes,[3] or polymer electrolytes.[4] However, these alternatives, still face some challenges for example, most polymer electrolytes often exhibit insufficient room temperature ionic conductivities, while the large interfacial resistance and high rigidity of inorganic solid electrolytes restrict their application in flexible batteries.

Besides inorganic solid electrolytes and polymer electrolytes, aqueous electrolytes have been considered as a promising choice for flexible and wearable electronics,[5] since they are non-flammable, environmentally benign, and cost effective. In particular, hydrogel electrolytes that are composed of elastic cross-linked polymer and aqueous electrolyte, are mechanically strong and soft and can be used in flexible energy storage devices as both electrolyte and separator.[6] For the realization of hydrogel electrolytes with an extended electrochemical stability window (ESW), highly concentrated aqueous electrolytes (such as "water-in-salt,"[7] and "water-in-bisalt"[8] electrolytes) were introduced. For example, Chen et al. reported the use of a polyacrylamide (PAM)- "water-in-salt" electrolyte in a stretchable solid-state LIB.[7b] This hydrogel electrolyte offers high ionic conductivity as well as mechanical flexibility. Spencer et al. introduced "water-in-bisalt" electrolyte into an acrylic polymer. Benefiting from the strong coordination of water with abundant hydrophilic functional group in the polymer chain, the ESW of this electrolyte was extended further, and it could enable the cycling of an aqueous LIB with a lithium titanate anode ($Li_4Ti_5O_{12}$, LTO).[8] However, the inevitable hydrogen evolution reaction (HER) at low potential leads to severe capacity fading, restricting the practical application of these hydrogel electrolytes.

Since the first report on eutectic electrolytes,[9] deep eutectic solvents (DESs) have garnered increasing attention in various batteries (i.e., Li,[10] Al,[11] and Zn[12] batteries) and supercapacitors,[13] owing to their unique properties of low vapor pressure, low cost, wide liquid range, high thermal stability, and broad ESW. When applying in battery systems, DESs are commonly prepared by mixing Lewis acids (e.g., metal chlorides $ZnCl_2$ and $AlCl_3$) with protic Lewis bases (urea, acetamide, N-methylacetamide, etc.).[14] Eutectogels (ETGs), a potential electrolyte candidate for quasi-solid-state aqueous LIBs, then can be obtained by the polymerization of monomers that dissolved in the DESs.[15] Despite the high safety and better electrochemical stability, ETGs still suffer from low ionic conductivity.

Because of the small size of the water molecule and its miscibility with DESs,[16] we consider that water would be able to address the conductivity and flexibility issues of ETGs. Through the introduction of small amounts of water, the physicochemical properties of DES may be improved (e.g., enhancing ionic conductivity) while maintaining the broad ESW of ETGs. Thus, we herein introduce "water-in-ETG" (WiETG) electrolytes as a new class of quasi-solid-state electrolyte in which water acts as a plasticizer and enables DES uptake by the polymer. WiETGs are prepared via swelling a hydrogel polymer with DES with low water content. Compared with "water-in-salt" electrolytes, the water molecules tend to be isolated in ETGs,[12a] which prevents hydrogen evolution at the anode|electrolyte interface. This study provides a new perspective for the use of water in quasi-solid-state aqueous energy storage system.

2. Results and Discussions

2.1. Physicochemical Properties of WiETG Electrolytes

A carboxymethyl cellulose (CMC)-cross-linked PAM polymer that possesses good mechanical strength and thermal stability was chosen as the polymer backbone.[17] It was fabricated via free-radical polymerization of acrylamide (AM) with a cross-linker in aqueous CMC solution. The PAM chains form a network by covalent cross-links. Meanwhile, the –C=O (or –OH) groups on CMC chains bond (through hydrogen bonds) with the $-CONH_2$ groups on the PAM chains (**Figure 1**a), resulting in a mechanically stretchable and tough hydrogel. The dry polymer membrane was obtained via freeze-drying, which allowed keeping the structure of the polymer framework. SEM images of the cross section and top view of the dry polymer are shown in Figure 1d,e, respectively. The cross-linked polymer with a thickness of ≈100 µm displays a gradually increasing pore size with a range of 2 to 20 µm from the surface to the center (Figure 1d), which is beneficial for the uptake of liquid electrolytes. Moreover, a smooth surface can be seen from the top view (Figure 1e).

WiETG electrolytes were prepared by immersing the dry polymer into DES electrolytes with different contents of water (n_{LiTFSI}: $n_{acetamide}$: n_{H2O} = 1:3:x, x = 0, 0.5, 1, and 2, that are noted as ACE0, ACE05, ACE1, and ACE2, respectively. The physicochemical properties of DES electrolytes are shown in Table S1, Supporting Information). However, as shown in Figure S1, Supporting Information, when immersing in ACE0 and ACE05, only limited liquid electrolyte was absorbed by the polymer due to the weak hydrogen bond between DES and polymer chain. On the contrary, benefiting from the strong hydrogen bonds between water and the $-CONH_2$ and –OH groups from the polymer chains, the absorption of DES into the polymer was increased with higher water content, resulting in WiETG electrolyte formation (Figure 1b). Finally, a transparent film was obtained after immersing the dry polymer in ACE1 (Figure 1c) or ACE2, noted as CP-131 and CP-132, respectively. The "water-in-salt" gel polymer electrolyte (GPE) was also prepared for comparison, by immersing the same dry polymer into 21 mol kg^{-1} LiTFSI and was noted as CP-21m.

The Li^+-acetamide-H_2O interactions in the DES and WiETG electrolytes were investigated using Fourier transform infrared spectroscopy (FTIR) (Figure 1g; Figures S2, S3, Supporting Information). As shown in Figure 1g, the two strong band at 3155 and 3307 cm^{-1} are assigned to symmetric stretching ($\nu_s(NH_2)$) and asymmetric stretching ($\nu_{as}(NH_2)$) vibrations of N–H in acetamide, respectively. For the spectra of ACE0, CP-131, and CP-132, the peaks of these two vibrations shift toward higher wavenumber (3374 and 3466 cm^{-1}, respectively) because the hydrogen bonds are weakened in acetamide, which is caused by the participation of acetamide in Li^+ solvation shell (Figure 1f).[18] No obvious vibration shift was found with the water content increase, suggesting that the acetamide was kept in the solvation shell rather than replaced by water molecular. It indicates that the stronger interaction between acetamide and Li^+ than H_2O with Li^+, which was further confirmed by DFT results. Additionally, contrary to the ACE0 electrolyte, a new broad band located at 3586 cm^{-1} is observed in the spectra of

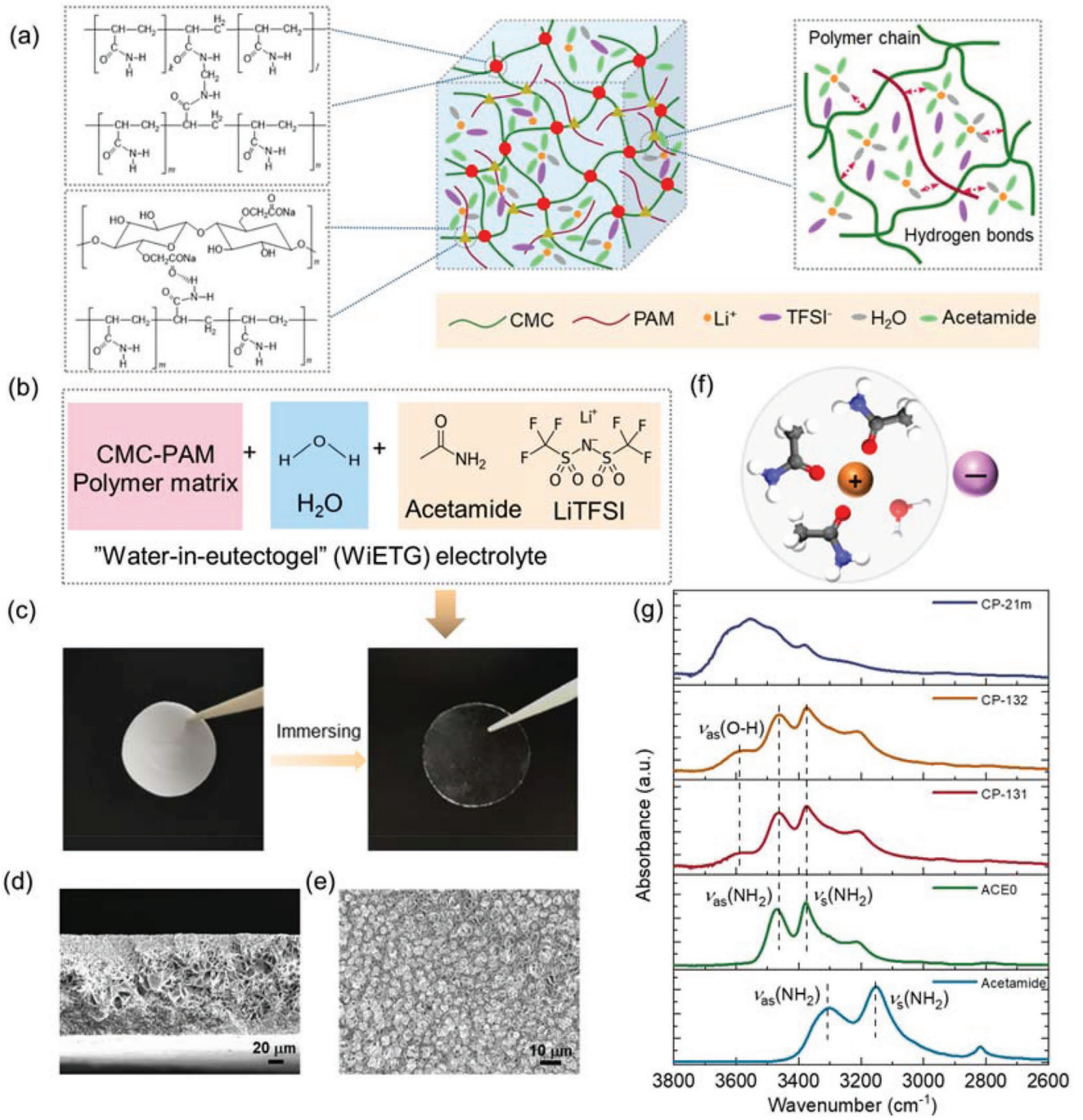

Figure 1. a) Schematic illustration of the chemical bonds and hydrogen bonds in WiETGs. b) Compositions of WiETG electrolytes. c) Image of CMC-PAM polymer after freeze-drying and after immersing in ACE-131 electrolyte. SEM images of the d) cross section and e) top view of the CMC-PAM polymer membrane after freeze-drying. f) Illustration of the Li^+ primary solvation shell in the ACE1 electrolyte (H, white; Li, orange; C, Grey; N, blue; O, red; TFSI, purple). g) FTIR spectra of acetamide, ACE0, CP-131, CP-132, and CP-21m in the range of 2600 to 3800 cm^{-1}.

CP-131 and CP-132, which is assigned to chemically bonded water ($\nu_{as}(H_2O)$). It indicates that isolated water interacted with acetamide, which is consistent with previous reports.[12a,19]

Liquid electrolyte uptake by the polymer host is a critical property for the ionic conductivity of GPEs. As shown in **Figure 2**a and Table S2, Supporting Information, the CP-21m reveals an abundant electrolyte uptake of ≈3600 wt%. As for CP-131 and CP-132, the electrolyte uptake decreased to 1500 wt%, which is still very high compared with conventional GPEs. Moreover, the water-retention under ambient conditions is also evaluated (relative humidity of ≈60%). Figure 2b shows that the mass of CP-132 decreases while that of CP-21m increases during the first day, and both remain nearly constant afterward. Moreover, the CP-131 weight changes are negligible

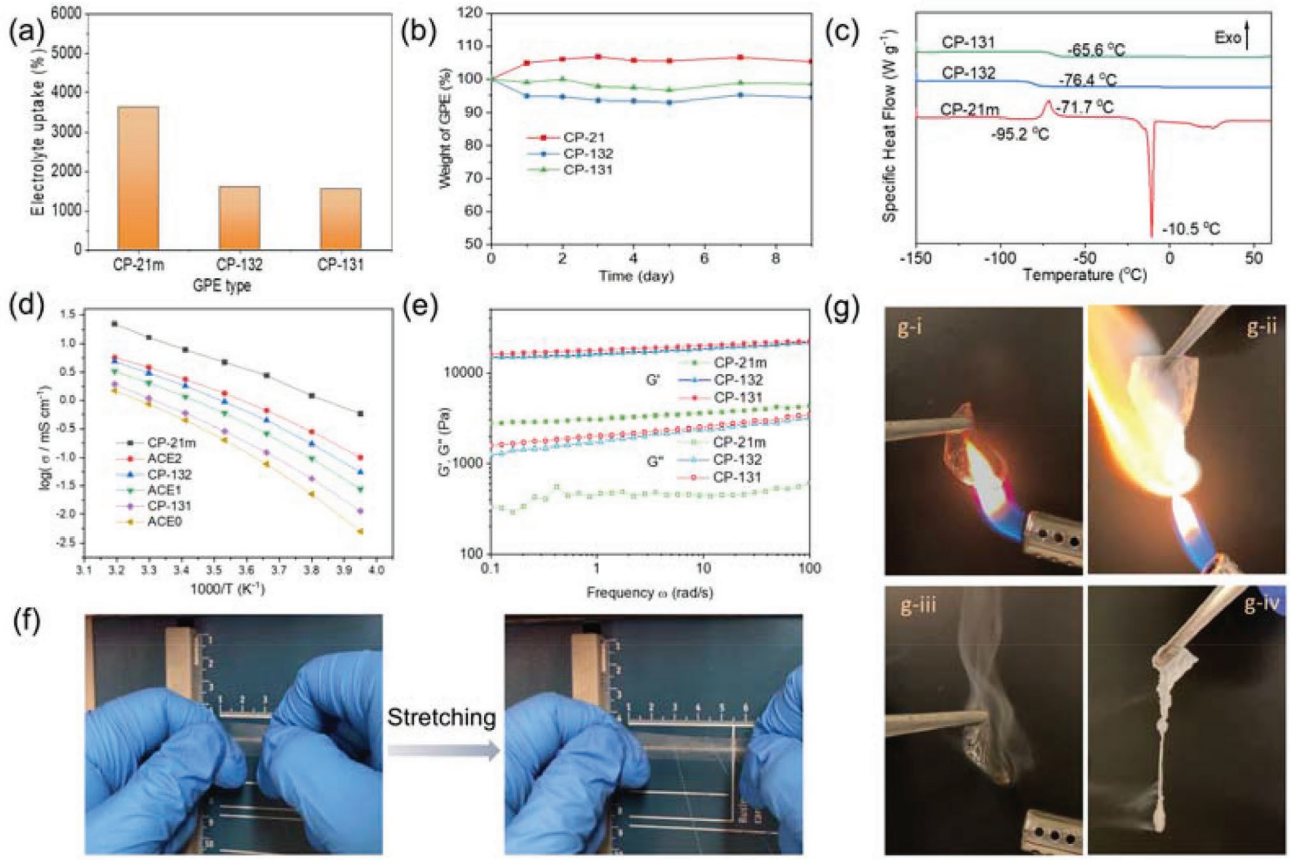

Figure 2. a) Liquid electrolyte uptake (wt%) and b) weight evolution of CP-131, CP-132, and CP-21m in the air at room temperature. c) The DSC curves of CP-131, CP-132, and CP-21m. d) Arrhenius plot of conductivities of various DES and WiETG electrolytes. e) Oscillatory shear rheology of the hydrogel electrolyte. The storage (G') and loss (G'') moduli are plotted as functions of the frequency ω. f) Photographs of the hydrogel electrolyte in the unstretched (left) and the stretched (right) states. g) Optical images of flame test on WiETG electrolyte (g-i,g-iii). For comparison, the LP 30 electrolyte with Celgard separator is tested as the reference (g-ii,g-iv).

even after 9 days, exhibiting a superior ability to maintain water inside the polymer. Thus, it indicates that WiETGs show good stability versus aqueous electrolyte under ambient environment.

The thermal stability of WiETGs was evaluated using differential scanning calorimetry (DSC) (Figure 2c; Figure S4, Supporting Information) and thermogravimetric analysis (TGA) (Figures S5, S6, Supporting Information). Similarly to the DSC curves of DES electrolytes, only one endothermic peak is obtained in DSC curves of CP-131 and CP-132 electrolytes which is attributed to the glass transition temperature (T_g) of WiETG.[15a] The low T_g of WiETGs indicate that the CP-131 and CP-132 remain in an amorphous phase across a wide temperature range. By comparison, the T_g of CP-21m is observed at –95.2 °C, while one exothermic peak (–71.7 °C) and an endothermic peak (–10.5 °C), are observed in CP-21m, which corresponds to the cold crystallization and melting of a crystalline phase, respectively. Three stages of weight loss can be observed in the TGA curves of as-prepared WiETGs, originating from the evaporation of water (<120 °C), the decomposition of acetamide or polymer species (120–400 °C), and the decomposition of LiTFSI (>400 °C), respectively. Therefore, WiETGs show high thermal stability across a wide temperature range.

The ionic conductivity Arrhenius plots of various WiETG and the related DES electrolytes are shown in Figure 2d. Apparently, similarly to DES electrolytes with water, the increase of water content results in the higher ionic conductivity of WiEGTs. The conductivity of the WiETG electrolyte decreases compared with the related DES electrolyte. It can be ascribed to the interaction between Li^+ solvation shell with polymer chain lowering the ion mobility. Although the ionic conductivity of CP-131 (1.08 mS cm^{-1} at 30 °C) is lower than "water-in-salt" polymer electrolyte CP-21m (12.8 mS cm^{-1} at 30 °C), it is higher than those of ACE0 (0.85 mS cm^{-1}) and typical solid polymer electrolytes.[20]

The dynamic mechanical properties of the WiETGs were investigated by oscillatory shear rheometry. Figure 2e presents the frequency (ω) response of the storage modulus (G') and loss modulus (G'') for CP-131, CP-132, and CP-21m GPEs. The storage moduli G' of all GPEs are much greater than their G'' and remain almost unchanged over the entire frequency range (0.1 to 100 rad s^{-1}), implying these electrolytes predominantly display an elastic behavior. Notably, CP-131 exhibits the highest G' and G'' values of 18 and 2 kPa (at 1 rad s^{-1}), respectively, owing to the enhanced hydrogen bond between CMC and PAM with reduced water content, which makes it strong enough to be used as separator. In addition, as depicted in Figure 2f and Video S1, Supporting Information, CP-131 shows good stretching ability even after extending to nearly 250% and it

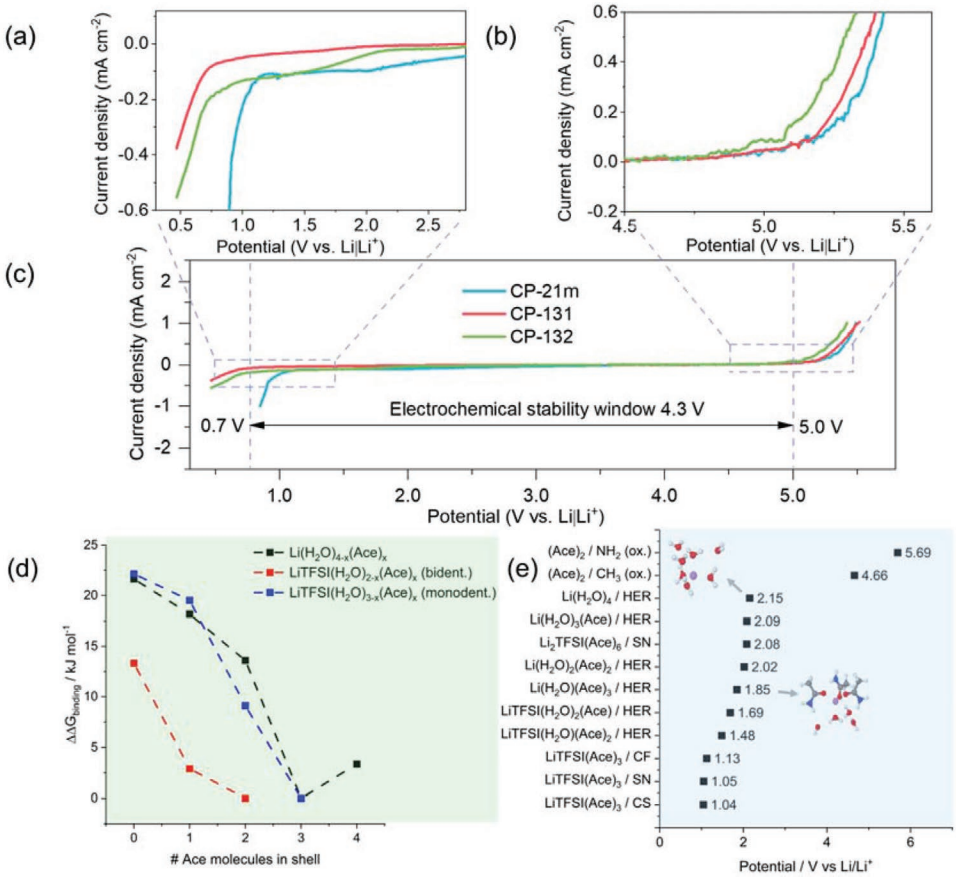

Figure 3. Electrochemical stability windows of CP-131, CP-132, and CP-21m. Magnified view of the regions near a) cathodic and b) anodic potential extremes in the c) overall curves. d) Relative binding free energies $\Delta\Delta G$ (in kJ mol^{-1}) for Li^+ solvate structures with $(H_2O)_{4-x}(Ace)_x$ solvation shells (black), Li^+ with $TFSI^-$ (monodentate) ion pair filled out with $(H_2O)_{3-x}(Ace)_x$ solvation shells (blue), and Li^+ with $TFSI^-$ (bidentate) ion pair filled out with $(H_2O)_{2-x}(Ace)_x$ solvation shells (red). A value > 0 indicates less favorable binding. e) Reduction and oxidation potentials computed for a number of relevant species. SN refers to TFSI decomposition by S-N cleavage, CS by C-S cleavage, and CF by C-F cleavage. HER denotes hydrogen evolution reaction; two structures are included which highlight a systematic addition of three waters in the 2nd solvation shell to stabilize the OH^- in the reduction product.

recovers its original shape when removing the force of deformation, demonstrating superior elasticity and flexibility.

The flammability of CP-131 was evaluated by exposing the gel polymer to a flame more than 5 s. A typical Celgard separator (type 2325) after immersion into an organic electrolyte LP30 (1 M $LiPF_6$ in ethylene carbonate: dimethyl carbonate 1:1 wt%) was used as reference. Typically, a sample is classified as "non-flammable" if the flame extinguished within 1 s after removing the flame.[21] As shown in Figure 2g, Videos S2, S3, Supporting Information, after removing the flame, contrary to the Celgard separator with LP30, CP-131 exhibits no flame, despite some charring of the membrane and signs of electrolyte boiling/overheating, demonstrating an excellent safety property owing to the intrinsically safe nature of each component.

2.2. Electrochemical Stability of WiETG Electrolytes

LSVs were conducted in a three-electrode cell configuration to evaluate the ESW of CP-131, CP-132, and CP-21m. As shown in **Figure 3**a–c, WiETG electrolytes and especially CP-131, show wider ESWs than "water-in-salt" GPEs. Anodic stabilities of CP-21m and CP-131 were extended to ≈5 V (vs Li|Li^+) as water oxidation is delayed by $TFSI^-$.[22] In a previous study, oxidization coupled with H transfer was identified in PAM residues above 4 V (vs Li|Li^+).[23] Similar processes were identified for acetamide as well occurring at 4.66 and 5.69 V (vs Li|Li^+) (Figure S7, Supporting Information).[24]

Moreover, CP-131 exhibits the smallest reduction current density and lowest reduction potential (0.7 V vs Li|Li^+) due to its lowest water content among the three electrolytes. In comparison with the DES electrolyte (Figure S8, Supporting Information), the reduction current density of ACE1 is higher than CP-131, suggesting that the coordination of water and DES molecules with the polymer chains suppresses the hydrogen evolution at low potential, which is consistent with literature.[7b,8] In conclusion, a broadened ESW of 4.3 V with low reduction potential below 1.0 V (vs Li|Li^+) is achieved for CP-131, which is sufficient to support the reversible lithiation/delithiation of $LiMn_2O_4$ (LMO) cathode (Figure S9, Supporting Information) and LTO anode (Figure S10, Supporting Information), respectively. However, the direct application of WiETGs in Li metal cells is still challenge due to the slow reaction between Li metal anode and water molecular in

them, as proved by the aging experiments (Figure S11, Supporting Information).

Density functional theory (DFT) calculations were performed to predict the relative binding free energies between Li^+ and LiTFSI ion pairs with water, acetamide, and mixed composition solvation shells (Figure 3d). In general, acetamide coordination to Li^+ is preferred over water although the binding free energies of $Li(H_2O)(Ace)_3$ versus $Li(Ace)_4$ show a small 2.90 kJ mol^{-1} preference for the mixed composition. Consequently, hydrogen evolution from $Li(H_2O)(Ace)_3$ shells is expected to be one of the limiting factors governing cathodic stability in the ACE1 and CP-131 electrolytes. To this end, DFT calculations were performed to estimate onset potentials for the HER evolved from shells with varying water content (Figure 3e). The Ace-free ($Li(H_2O)_4$) solvate has the highest HER potential (2.15 V vs $Li|Li^+$). A sizeable shift of HER from 2.15 to 1.85 V (vs $Li|Li^+$) ($Li(H_2O)(Ace)_3$) due to depolarization of the remaining water(s) in the solvation shell by the organic solvent. Previous molecular dynamics simulations have shown that 10–40% of Li^+ in 21 m LiTFSI-H_2O remains in this vulnerable $Li(H_2O)_4$ state, thus providing the impetus to alter these solvation shells further to suppress HER.[25] For those Li^+ involved in contact ion pairs and aggregates, the presence of $TFSI^-$ also partially depolarizes Li^+-bound water molecules, further suppressing HER even assuming higher water content. The DFT result is consistent with the trend in cathodic stabilities for CP-21m, CP-132, and CP-131 electrolytes (Figure 3a). Anion decomposition in $LiTFSI(Ace)_3$ solvation shells is also predicted to occur near 1.1 V (vs $Li|Li^+$) (Figure S12, Supporting Information, right side). The three major pathways for anion decomposition: defluorination (C-F cleavage), C-S cleavage, and S-N cleavage, were each found to have similar reduction potentials when originating from a neutral ion pair cluster. However, the formation of Li_xTFSI aggregates in solution (Figure S12, Supporting Information, top left) or induced by Li^+ accumulation near carbonyl sites of PAM results in reduction potentials in the range of 1.7–2.2 V (vs $Li|Li^+$).[23] The combination of high reduction potential for aggregate species and suppressed HER potential results in the rapid formation of robust SEI for CP-131 electrolytes, improving over the CP-21m electrolyte where HER and anion decomposition occur simultaneously.

Moreover, we also considered the chemical decomposition of $TFSI^-$ in Figure S12, Supporting Information (bottom left) as proposed by Dubouis and coworkers.[26] A previous theoretical investigation on the related triflate anion showed that while the reaction may be favored thermodynamically, there is a rather high barrier ≈215 kJ mol^{-1} (OH^- attacks CF_3) to overcome.[27] A smaller barrier of ≈105 kJ mol^{-1} was found for the SO_3 side, but attacking the sulfur appears hindered in $TFSI^-$ with very simple cluster calculations since it is difficult to isolate a sensible transition state. A more recent article investigated OH^- attack on the CF_3 group of $TFSI^-$ using metadynamics in solution to estimate a barrier of 298 kJ mol^{-1}.[28] In implicit solvent, we estimated the barrier to be 198.50 kJ mol^{-1} (not shown). However, the same reaction occurring in the $LiTFSI(H_2O)_3$ solvation shell has a barrier of 95.17 kJ mol^{-1}. Water is used here instead of acetamide or a mixed composition for computational expedience as transition state calculations tend to require more frequent calculation of expensive second derivatives. This result indicates chemical decomposition of TFSI may be another viable route to SEI formation.

2.3. Electrochemical Performance of WiETG Electrolytes

Full battery cells with LMO‖LTO configuration were constructed to examine the practical application of the hydrogel electrolytes. The cells are cycled between 1.00 and 2.75 V at 1 C (1 C = 150 mA g^{-1}). As shown in **Figure 4**a,b, a discharge capacity of 142 mAh g^{-1} is obtained in the cell with CP-131, which is obviously higher than that delivered from the cell with CP-21m (86 mAh g^{-1}), owing to limited side reactions during charge process in the full cell with CP-131. The energy efficiencies of LMO‖LTO full cells with CP131 and CP-21m were also compared. An energy efficiency of 86% is achieved by the cell with CP-131, but this value decreases to 34% for the cell with CP-21m due to the high overvoltage, suggesting an increased cost of the energy storage with CP-21m. The Coulombic efficiency (CE) and cycle stability of the cells with CP-131, CP-132, and CP-21m is presented in Figure 4c,d, respectively. The discharge capacity of the full cell with CP-21m decays rapidly to 9% of its initial capacity after 20 cycles and ultra-low CEs are obtained during the entire cycle life, demonstrating continuous side reactions in the cell. In the cell with the CP-132 electrolyte, due to dramatically decreased water content, the obtained discharge capacity is higher than for the cell with CP-21m, and the capacity is stable within 50 cycles. However, a decrease occurs afterward to 86 mAh g^{-1} in the 100th cycle. The CEs are much higher than those of the cell with CP-21m, but maintain a relatively low value of 93.5% during long-term cycling, likely originating from unstable SEI formation duo to the SEI components dissolution, cracking by gas bubbles, and continuous decomposition of electrolyte. With an even lower water content, the highest initial CE of 92.8% is achieved by the cell with CP-131. In addition, contrary to the cells with the other two electrolytes, the CE increases to 98.1% after 10 cycles, indicating the formation of an effective SEI in the first cycles. Most importantly, the discharge capacity remains at 119 mAh g^{-1} after 100 cycles, demonstrating a good cycling stability.

The good rate capability of the LMO‖LTO full cell with CP-131 is demonstrated in Figure 4e and Figure S13, Supporting Information. It delivers reversible capacities of 140, 113, 99, 86, 70, and 54 mAh g^{-1} at 1, 2, 3, 4, 5, and 6 C, respectively. When the current rate is returned to 1 C after the rate test, the cell delivers a capacity of 137 mAh g^{-1}, which is comparable to the initial capacity. When cycled at a high rate of 5 C, as shown in Figure 4f, the capacity retention is still 89% after 500 cycles, demonstrating an outstanding long-term cycling stability.

2.4. Post Mortem Analysis

To investigate the cycle stability of the SEI which contributes to cell resistance, EIS measurements were performed on an LMO‖LTO cell with CP-131 after 1, 5, and 10 cycles. As shown via the stable resistances shown in **Figure 5**a and Table S3, Supporting Information, an effective SEI, formed within the first five cycles, protects the electrode surface from

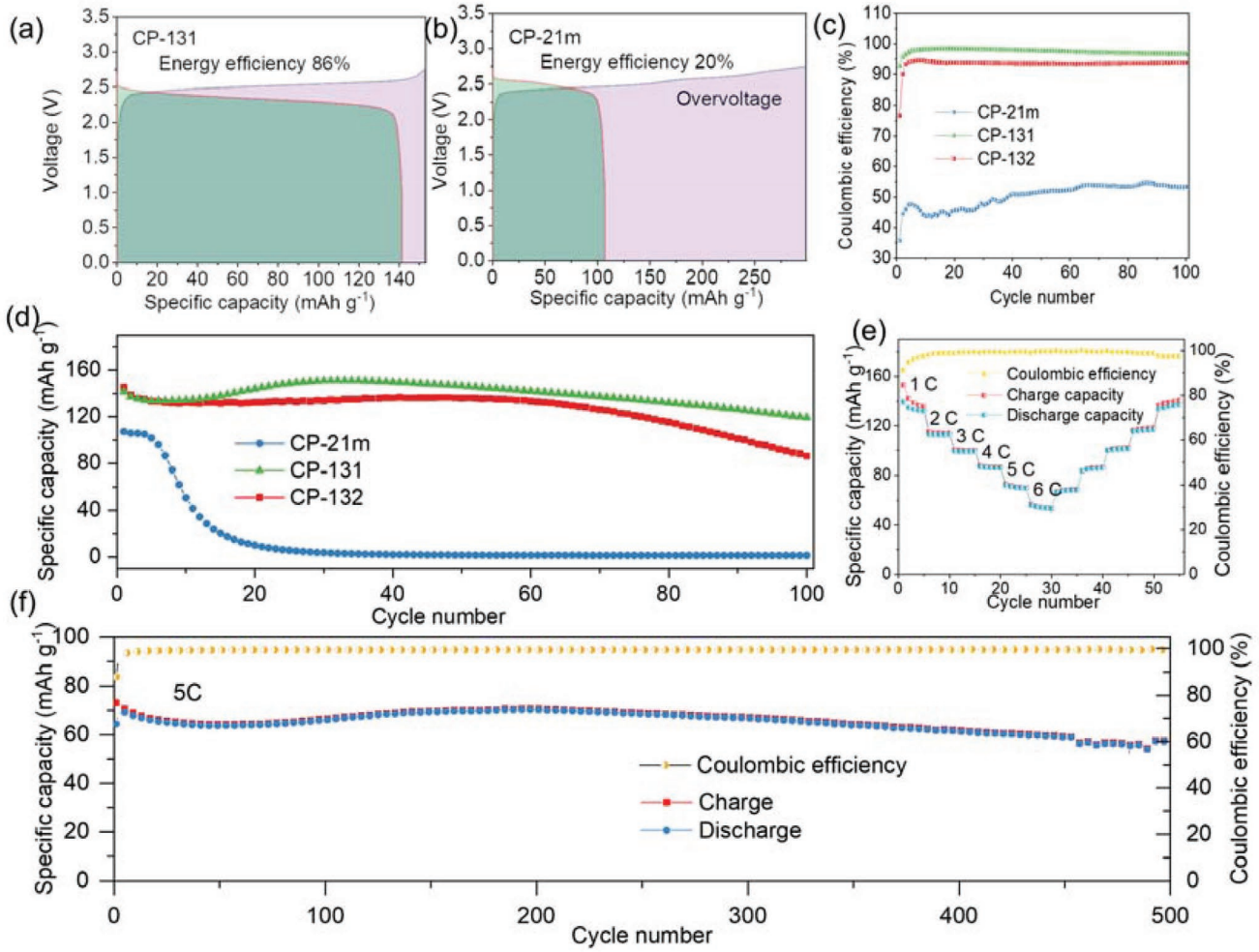

Figure 4. The voltage profiles of the first cycle of LMO||LTO full cell with a) CP-131 and b) CP-21m electrolyte. c) Coulombic efficiency and d) cycle performance of LMO||LTO full cell with CP-131, CP-132, and CP-21m at 1 C within the voltage range of 1.00–2.75 V. e) The rate performance of LMO||LTO full cell with CP-131 electrolyte varying from 1 to 6 C. f) Long-term cycling performance of LMO||LTO full cell with CP-131 at 5 C.

HER. Furthermore, the side reactions in LMO||LTO full cell with CP-131 was assessed by monitoring the change of open-circuit voltage (OCV) starting from a fully charged state after five completed cycles. As shown in Figure 5b, the OCV stabilizes at 2.41 V after 48 h, which further suggests a stable electrode-electrolyte interphase formation for the full cell with CP-131 electrolyte.

The compositions of SEI and cathode electrolyte interphase (CEI) formed on the electrodes in the LMO||LTO full cell with CP-131 electrolyte were then characterized by X-ray photoelectron spectroscopy (XPS). The F 1s, N 1s, and C 1s spectra of an LTO electrode were recorded after 100 cycles (Figure 5c). The signals of F 1s at 685.8 and 689.2 eV correspond to LiF and $-CF_3$, respectively, which originate from the reduction of the $TFSI^-$ anion. The decomposition products of $TFSI^-$ are also seen from the peaks of N 1s at 399.6 eV (-R-S-N-S species) and C 1s at 293.2 eV ($-CF_3$). As the OH^- originating from the reduction of H_2O contributes to the decomposition of LiTFSI,[26] the introduction of water to the DES electrolyte accelerates the formation of LiF on the anode surface. From the N 1s spectrum, a signal at 400.5 eV corresponding to $-CONH_2$ is detected, which is seen from the C 1s spectrum at 286.8 eV as well. According to previous work,[23] the $-CONH_2$ species derive from PAM and the PAM-rich electrode surface further suppresses hydrogen evolution and minimizes the dissolution of the SEI. Besides, the signal of C 1s at 289.8 eV corresponding to Li_2CO_3 is also observed as for the SEI formation in "water-in-salt" electrolytes. The formation of multi-compound SEI can effectively block the water decomposition during cycling. Regarding the surface of LMO electrode, as shown in Figure 5d, the $-CF_3$, –RSNS species, and LiF from the decomposition of LiTFSI are also detected. Combined with the oxidation product of acetamide and Li_2CO_3, a CEI film is formed on the LMO surface.

The morphologies of SEI and CEI were further investigated via SEM (Figures S15, S16, Supporting Information) and TEM (Figure 5e,f) respectively. After 100 cycles, a clear and smooth surface is observed on LTO electrode (Figure S16, Supporting Information) with a distinctively uniform and amorphous film of ≈6 nm (Figure 5e). Besides, a smooth and uniform CEI layer of ≈8 nm is seen on LMO surface (Figure 5f), which likely hinders the dissolution of transition metals and the oxygen evolution on electrode surface. Therefore, the thin SEI and CEI film formed on both anode and cathode surface can not only extend

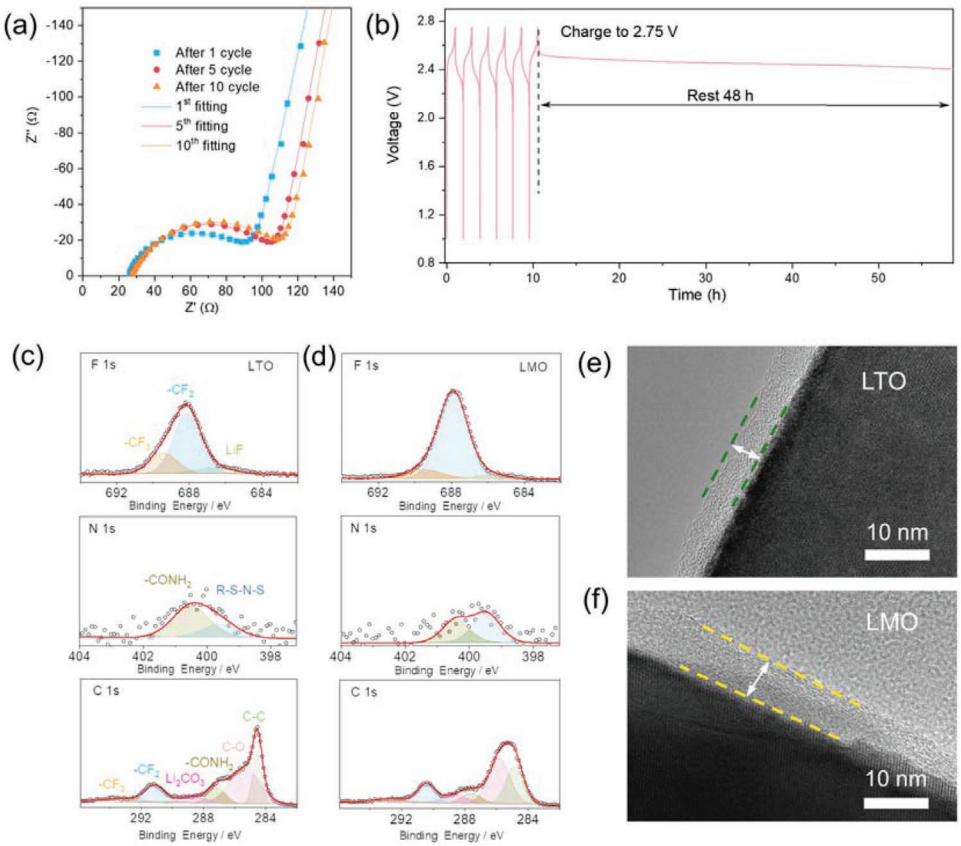

Figure 5. a) Nyquist plots of LMO||LTO full cell with CP-131 after cycling 1, 5, and 10 cycles. The equivalent circuit for fitting is shown in Figure S14, Supporting Information. b) Open circuit voltages (OCV) decays with rest time for LMO||LTO full cell with CP-131. The cell was rested at 100% SOC after 5 cycles between 1.00 and 2.75 V at 1 C. c,d) XPS patterns and e,f) HRTEM of LTO (c,e) and LMO (d,f) electrodes after cycling in the LMO||LTO full cell with CP-131 after 100 cycles, respectively.

the ESW but also allow fast Li^+ ion transport from the electrolyte to the electrode, which plays a critical role on the long-term cycling stability of batteries.

2.5. Electrochemical Performance of Flexible Battery Cells

The CP-131 WiETG was used to prepare an LMO||LTO pouch cell, using stainless steel mesh and aluminum mesh as cathode and anode current collector, respectively. The cycling performance is shown in **Figure 6**a. A capacity of 2.2 mAh is reached with a high CE of 90% for the first cycle at 1 C, and the capacity retention reaches ≈88% after 100 cycles. The charge/discharge voltage plateaus are stable and without marked overvoltage during cycling, demonstrating low inner resistance of the cell and a good interfacial stability among different components (Figure 6b). The flexibility of this quasi-solid-state battery was then evaluated by cycling the cell at different bending angles, and the cycling performance are shown in Figure 6c and Figure S17, Supporting Information. Only minor capacity and voltage plateaus changes occur after several cycles at 45°, 90°, 135°, and 180°, indicating its high potential to be used in flexible electronics. The temperature-dependent cycle performance of LMO||LTO pouch cell with CP-131 was also evaluated in a temperature range of −20 to 20 °C (Figure 6d). The discharge capacities of 120, 80, and 40 mAh g^{-1} are obtained at 0, −10, and −20 °C, respectively, showing good low temperature performance. Furthermore, the battery can be bent into various shapes without OCV change and continually power an LED light even in the extreme cases of being folded and cut (Figure 6e; Figure S18, Video S4, Supporting Information).

3. Conclusion

A new class of "water-in-eutectogel" electrolytes (WiETGs) is created to support quasi-solid-state aqueous lithium ion batteries. The obtained WiETGs exhibit both high safety and superior elastic properties in comparison with other polymer contained electrolyte, as summarized in radar plots (Figure S19, Supporting Information). Meanwhile, with water molecules participating in the Li^+ solvation structure in eutectic solvent, faster Li ion transport is achieved, resulting in enhanced ionic conductivity. Benefiting from the low water activity in WiETG electrolyte that is confirmed by DFT modeling, a relatively low reduction potential limit is obtained that enable the utilization of LTO anode. Moreover, LMO||LTO full battery cells

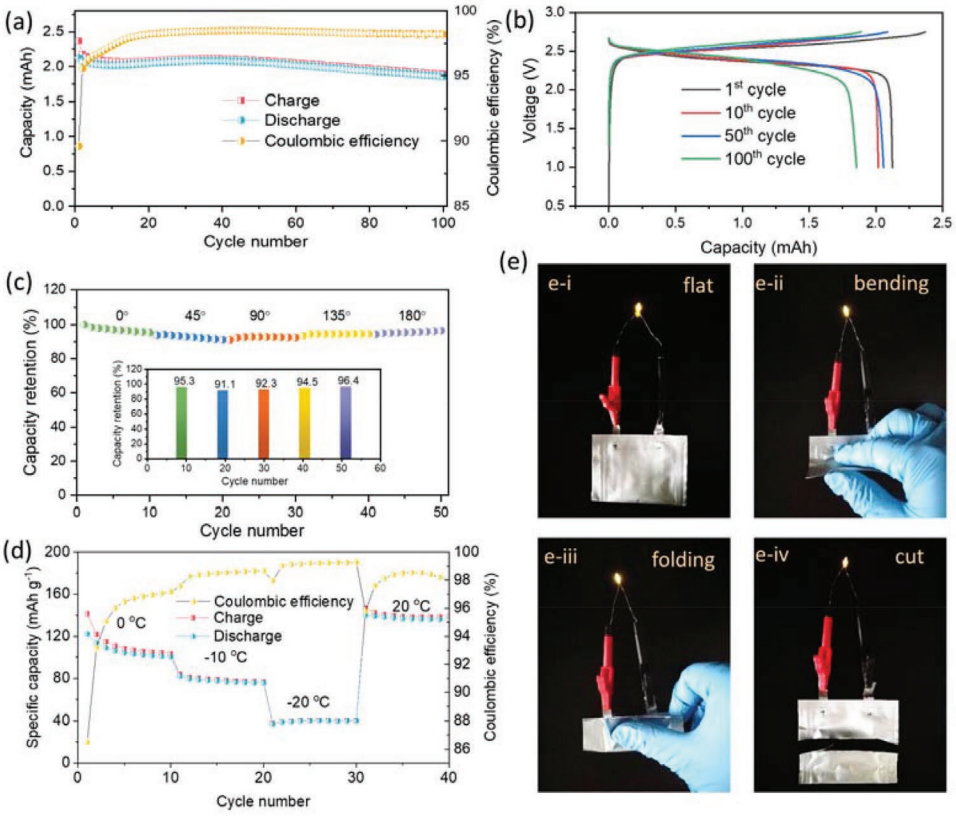

Figure 6. Electrochemical performance of LMO||LTO pouch cell with CP-131. a) Cycling stability and b) voltage profiles of 1, 10, 50, and 100 cycles within the range of 1.00 to 2.75 V at 1 C. c) The cycling performance under different bending angles from 0 to 180°. d) Electrochemical performance at different temperature ranging from –20 to 20 °C. e) Photograph of pouch cell connected in a LED light when being e-i) flat, e-ii) bended, e-i) folded, and e-iv) cut.

with CP-131 electrolyte exhibits high energy efficiency (86%, 1 C) and good cycle stability (89% retention after 500 cycles at 5 C), owing to effective SEI and CEI formation during the initial charge/discharge cycles that suppress HER effectively. A flexible LMO||LTO pouch cell with CP-131 electrolyte shows similar cycle capability to the corresponding coin cells even at different bending angles. A capacity retention of 86% is maintained at 0 °C, demonstrating wide range of service temperature. These results highlight that WiETGs electrolytes have the potential to be widely used for high-safety flexible electronic devices.

Supporting Information

Supporting Information is available from the Wiley Online Library or from the author.

Acknowledgements

X.H. and T.P.P. contributed equally to this work. The authors would like to acknowledge financial support from the European Union through the Horizon 2020 framework program for research and innovation within the projects "SPIDER" (814389), "VIDICAT" (829145), and Energy of the State of North Rhine-Westphalia (MWIDE, Germany) within the project "GrEEn" (313-W044A). Modeling work at Army Research Laboratory was supported by the Joint Center for Energy Storage Research, an Energy Innovation Hub funded by the US Department of Energy under cooperative agreement no. W911NF-19-2-0046.

Open Access Funding provided by Politecnico di Milano within the CRUI-CARE Agreement.

Conflict of Interest

The authors declare no conflict of interest.

Data Availability Statement

The data that support the findings of this study are available from the corresponding author upon reasonable request.

Keywords

aqueous lithium-ion batteries, quasi-solid-state electrolytes, water-in-eutectogel

Received: January 31, 2022
Revised: April 7, 2022
Published online: May 6, 2022

[1] a) T. Tao, S. Lu, Y. Chen, *Adv. Mater. Technol.* **2018**, *3*, 1700375; b) Z. Fang, J. Wang, H. Wu, Q. Li, S. Fan, J. Wang, *J. Power Sources* **2020**, *454*, 227932.

[2] a) L. Zeng, L. Qiu, H.-M. Cheng, *Energy Storage Mater.* **2019**, *23*, 434; b) H. Cha, J. Kim, Y. Lee, J. Cho, M. Park, *Small* **2018**, *14*, 1702989.
[3] T. Famprikis, P. Canepa, J. A. Dawson, M. S. Islam, C. Masquelier, *Nat. Mater.* **2019**, *18*, 1278.
[4] P. Yao, H. Yu, Z. Ding, Y. Liu, J. Lu, M. Lavorgna, J. Wu, X. Liu, *Front. Chem.* **2019**, *7*, 522.
[5] a) C. Yang, X. Ji, X. Fan, T. Gao, L. Suo, F. Wang, W. Sun, J. Chen, L. Chen, F. Han, *Adv. Mater.* **2017**, *29*, 1701972; b) W.-J. Song, S. Lee, G. Song, H. B. Son, D.-Y. Han, I. Jeong, Y. Bang, S. Park, *Energy Storage Mater.* **2020**, *30*, 260.
[6] Z. Wang, H. Li, Z. Tang, Z. Liu, Z. Ruan, L. Ma, Q. Yang, D. Wang, C. Zhi, *Adv. Funct. Mater.* **2018**, *28*, 1804560.
[7] a) J. Zhang, C. Cui, P.-F. Wang, Q. Li, L. Chen, F. Han, T. Jin, S. Liu, H. Choudhary, S. R. Raghavan, N. Eidson, A. von Cresce, L. Ma, J. Uddin, D. Addison, C. Yang, C. Wang, *Energy Environ. Sci.* **2020**, *13*, 2878; b) X. Chen, H. Huang, L. Pan, T. Liu, M. Niederberger, *Adv. Mater.* **2019**, *31*, 1904648.
[8] S. A. Langevin, B. Tan, A. W. Freeman, J. C. Gagnon, C. M. Hoffmanjr , M. W. Logan, J. P. Maranchi, K. Gerasopoulos, *Chem. Commun.* **2019**, *55*, 13085.
[9] A. P. Abbott, G. Capper, D. L. Davies, H. L. Munro, R. K. Rasheed, V. Tambyrajah, *Chem. Commun.* **2001**, *19*, 2010.
[10] a) A. Boisset, S. Menne, J. Jacquemin, A. Balducci, M. Anouti, *Phys. Chem. Chem. Phys.* **2013**, *15*, 20054; b) T. T. A. Dinh, T. T. K. Huynh, L. T. M. Le, T. T. T. Truong, O. H. Nguyen, K. T. T. Tran, M. V. Tran, P. H. Tran, W. Kaveevivitchai, P. M. L. Le, *ACS Omega* **2020**, *5*, 23843; c) Z. Hu, F. Xian, Z. Guo, C. Lu, X. Du, X. Cheng, S. Zhang, S. Dong, G. Cui, L. Chen, *Chem. Mater.* **2020**, *32*, 3405; d) Y. Hu, H. Li, X. Huang, L. Chen, *Electrochem. Commun.* **2004**, *6*, 28.
[11] a) W. Chu, X. Zhang, J. Wang, S. Zhao, S. Liu, H. Yu, *Energy Storage Mater.* **2019**, *22*, 418; b) M. Li, B. Gao, C. Liu, W. Chen, Z. Shi, X. Hu, Z. Wang, *Electrochim. Acta* **2015**, *180*, 811; c) L. Zhang, C. Zhang, Y. Ding, K. Ramirez-Meyers, G. Yu, *Joule* **2017**, *1*, 623.
[12] a) J. Zhao, J. Zhang, W. Yang, B. Chen, Z. Zhao, H. Qiu, S. Dong, X. Zhou, G. Cui, L. Chen, *Nano Energy* **2019**, *57*, 625; b) H. Qiu, X. Du, J. Zhao, Y. Wang, J. Ju, Z. Chen, Z. Hu, D. Yan, X. Zhou, G. Cui, *Nat. Commun.* **2019**, *10*, 5374.
[13] W. Zaidi, A. Boisset, J. Jacquemin, L. Timperman, M. Anouti, *J. Mater. Chem. C* **2014**, *118*, 4033.
[14] E. L. Smith, A. P. Abbott, K. S. Ryder, *Chem. Rev.* **2014**, *114*, 11060.
[15] a) B. Joos, T. Vranken, W. Marchal, M. Safari, M. K. Van Bael, A. T. Hardy, *Chem. Mater.* **2018**, *30*, 655; b) S. Hong, Y. Yuan, C. Liu, W. Chen, L. Chen, H. Lian, H. Liimatainen, *J. Mater. Chem. C* **2020**, *8*, 550; c) B. Joos, J. Volders, R. R. da Cruz, E. Baeten, M. Safari, M. K. Van Bael, A. T. Hardy, *Chem. Mater.* **2020**, *32*, 3783; d) C. Zhang, Z. Niu, J. Bae, L. Zhang, Y. Zhao, G. Yu, *Energy Environ. Sci.* **2021**, *14*, 931.
[16] a) O. S. Hammond, D. T. Bowron, K. J. Edler, *Angew. Chem., Int. Ed.* **2017**, *56*, 9782; b) N. López-Salas, J. M. Vicent-Luna, S. Imberti, E. Posada, M. A. J. S. Roldán, J. A. Anta, S. R. Balestra, R. M. Madero Castro, S. Calero, R. J. Jiménez-Riobóo, *ACS Sustainable Chem. Eng.* **2019**, *7*, 17565.
[17] F. Lin, X. Lu, Z. Wang, Q. Lu, G. Lin, B. Huang, B. Lu, *Cellulose* **2019**, *26*, 1825.
[18] a) T. Theophanides, P. D. Harvey, *Coord. Chem. Rev.* **1987**, *76*, 237; b) Y. Hu, Z. Wang, H. Li, X. Huang, L. Chen, *Spectrochim. Acta, Part A* **2005**, *61*, 2009.
[19] J. Xu, X. Ji, J. Zhang, C. Yang, P. Wang, S. Liu, K. Ludwig, F. Chen, P. Kofinas, C. Wang, *Nat. Energy* **2022**, *7*, 186.
[20] Q. Zhang, K. Liu, F. Ding, X. Liu, *Nano Res.* **2017**, *10*, 4139.
[21] S. Hess, M. Wohlfahrt-Mehrens, M. Wachtler, *J. Electrochem. Soc.* **2015**, *162*, A3084.
[22] L. Suo, O. Borodin, T. Gao, M. Olguin, J. Ho, X. Fan, C. Luo, C. Wang, K. Xu, *Science* **2015**, *350*, 938.
[23] X. Hou, R. Wang, X. He, T. P. Pollard, X. Ju, L. Du, E. Paillard, H. Frielinghaus, L. C. Barnsley, O. Borodin, *Angew. Chem., Int. Ed.* **2021**, *60*, 22812.
[24] a) X. Liu, Z. Yu, E. Sarnello, K. Qian, S. Seifert, R. E. Winans, L. Cheng, T. Li, *Energy Mater. Adv.* **2021**, *2021*, 7368420; b) M. Berholts, H. Myllynen, K. Kooser, E. Itälä, S. Granroth, H. Levola, J. Laksman, S. Oghbaiee, B. Oostenrijk, E. Nõmmiste, *J. Chem. Phys.* **2017**, *147*, 194302.
[25] a) O. Borodin, L. Suo, M. Gobet, X. Ren, F. Wang, A. Faraone, J. Peng, M. Olguin, M. Schroeder, M. S. Ding, E. Gobrogge, A. von Wald Cresce, S. Munoz, J. A. Dura, S. Greenbaum, C. Wang, K. Xu, *ACS Nano* **2017**, *11*, 10462; b) Y. Zhang, N. H. C. Lewis, J. Mars, G. Wan, N. J. Weadock, C. J. Takacs, M. R. Lukatskaya, H.-G. Steinrück, M. F. Toney, A. Tokmakoff, E. J. Maginn, *J. Phys. Chem. B* **2021**, *125*, 4501.
[26] N. Dubouis, P. Lemaire, B. Mirvaux, E. Salager, M. Deschamps, A. Grimaud, *Energy Environ. Sci.* **2018**, *11*, 3491.
[27] L. Cao, D. Li, T. Pollard, T. Deng, B. Zhang, C. Yang, L. Chen, J. Vatamanu, E. Hu, M. J. Hourwitz, L. Ma, M. Ding, Q. Li, S. Hou, K. Gaskell, J. T. Fourkas, X.-Q. Yang, K. Xu, O. Borodin, C. Wang, *Nat. Nanotech.* **2021**, *16*, 902.
[28] A. France-Lanord, F. Pietrucci, A. M. Saitta, J.-M. Tarascon, A. Grimaud, M. Salanne, (Preprint) https://doi.org/10.26434/chemrxiv-2021-x7z1v (submitted: December 2021).